JOURNAL OF GEOPHYSICAL RESEARCH, VOL. 115, A06301, doi:10.1029/2009JA014752, 2010

A kinetic ballooning/interchange instability in the magnetotail

P. L. Pritchett[1] and F. V. Coroniti[1]

Received 10 August 2009; revised 3 December 2009; accepted 4 January 2009; published 8 June 2010.

[1] Three-dimensional electromagnetic particle-in-cell simulations are used to investigate the stability properties of a plasma sheet equilibrium with a minimum in the magnetic normal (B_z) component. Such a configuration is found to be unstable to a ballooning/interchange type mode that is localized tailward of the B_z minimum. The mode has a relatively short dawn-dusk wavelength of the order of the ion Larmor radius in the B_z field (~2000 km) and a phase velocity in the direction of the ion diamagnetic drift with a magnitude about one-fifth of the drift speed. The real frequency is about 60% of the midplane ion cyclotron frequency. The dominant mode polarization is $\delta\phi$ and $\delta B_{\|}$. A linear kinetic analysis including bounce and drift resonance interactions for the electrons and an orbit average over the flux tube volume for the Boltzmann term in the ion density perturbation produces agreement with the simulation mode properties and permits identification of the mode as the low-frequency extension of the lower hybrid drift instability in straight magnetic geometry. In its nonlinear evolution, the mode develops Rayleigh-Taylor fingers that extend across the B_z minimum and into the near-Earth dipole region. These fingers transport magnetic flux earthward, and the flux is redistributed by electron Hall currents that flow around the fingers. This mode is likely to contribute to the nearly continuous presence of turbulence in the center of the plasma sheet.

Citation: Pritchett, P. L., and F. V. Coroniti (2010), A kinetic ballooning/interchange instability in the magnetotail, *J. Geophys. Res.*, *115*, A06301, doi:10.1029/2009JA014752.

1. Introduction

[2] Despite the continued controversy concerning the physical processes and time sequences involved in the onset of substorms [e.g., *Baker et al.*, 1996; *Lui*, 1996], there is general agreement that the growth phase begins with the initiation of dayside reconnection following a southward IMF shift. This process removes closed magnetic flux from the dayside and transports open flux into the magnetotail. The resulting increase in solar wind stress should then initiate a period of enhanced internal convection in the tail [*Coroniti and Kennel*, 1973].

[3] The understanding of this convection stage also has had a long history. *Erickson and Wolf* [1980] argued that steady, adiabatic convection probably could not occur throughout a closed field line region extending into a long magnetotail. They demonstrated that if one takes a typical plasma sheet flux tube extending to 60 R_E and adiabatically compresses it to a volume typical of a 10 R_E flux tube, then the resulting pressure is too large by an order of magnitude to be confined by the observed magnetic field (the "pressure balance inconsistency"). This effect was confirmed by *Schindler and Birn* [1982]. Modeling the adiabatic convection of plasma sheet flux tubes as a series of static equilibrium solutions in which PV^{γ} was conserved, *Erickson* [1984] found that the enhanced pressure led to the formation of a deep minimum in the equatorial field B_z in the inner plasma sheet. Explicit force-balanced magnetic field models in two dimensions with constant PV^{γ} likewise exhibited a stressed configuration with a magnetic field minimum [*Hau et al.*, 1989; *Hau*, 1991; *Erickson*, 1992]. While not a feature of statistical observations [e.g., *Fairfield*, 1986], such midtail minima have been observed during periods of extended magnetospheric convection [*Sergeev et al.*, 1994]. In addition, the enhanced pressure in the near-Earth plasma sheet was found to choke the incipient earthward convection and to lead to the formation of a thin electron-dominated current sheet [*Pritchett and Coroniti*, 1995]. Observation of such thin current sheets has by now been reported on many occasions [*Mitchell et al.*, 1990; *Sergeev et al.*, 1993; *Sanny et al.*, 1994; *Pulkkinen et al.*, 1994; *Pulkkinen and Wiltberger*, 2000; *Mozer et al.*, 2002; *Asano et al.*, 2003, 2004; *Wygant et al.*, 2005].

[4] The presence of a deep B_z minimum in the midtail suggests several mechanisms that could lead to disruption of the tail. Such a configuration could be tearing mode unstable [*Hau et al.*, 1989], or the continued driving by the convection field could force B_z through zero and thus initiate reconnection [*Pritchett and Coroniti*, 1990; *Pritchett et al.*, 1997]. Alternatively, such a configuration could drive various interchange processes. It has long been recognized that

[1]Department of Physics and Astronomy, University of California, Los Angeles, California, USA.

0148-0227/10/2009JA014752

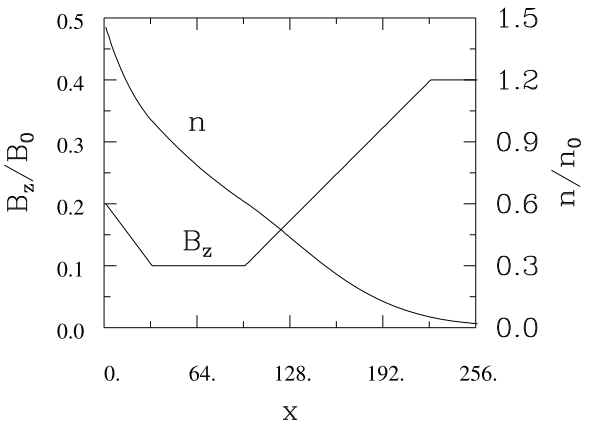

Figure 1. Initial equilibrium profiles in the equatorial plane for the magnetic field $B_{0z}(x, 0)$ (left-hand scale) and the density $n(x, 0)$ (right-hand scale).

the curvature of the magnetic field in a magnetized plasma can play the role of an effective gravitational force and excite a Rayleigh-Taylor (RT) type instability [*Rosenbluth and Longmire*, 1957]. The modifications to the basic RT instability that occur when the ion gyrofrequency and ion gyroradius become important have been considered for the case of a straight magnetic field geometry in the Hall MHD model [e.g., *Huba et al.*, 1987] and in the hybrid model which retains full kinetic ion dynamics while treating the electrons as a massless fluid [e.g., *Winske*, 1996].

[5] Within an explicit magnetotail configuration, a number of interchange models have been investigated. *Pontius and Wolf* [1990] suggested the existence of plasma depletions ("bubbles") in the plasma sheet. These bubbles should convect earthward due to a buoyancy effect and would thus lead to a reduction in plasma content. This effect would tend to ease the pressure balance inconsistency. *Chen and Wolf* [1993] extended this idea and suggested that such bubbles could be the source of the bursty bulk flows observed in the tail [*Baumjohann et al.*, 1990; *Angelopoulos et al.*, 1992]. *Pritchett and Coroniti* [1997] used a 3-D particle simulation to model the convection process in the plasma sheet. Using a tailward boundary condition that prevented magnetic flux from leaving the system led to the dynamical formation of a tailward gradient region in the equatorial field profile that was unstable to an interchange mode with wavelength of 1–2 R_E ($k_y\rho_{in} \sim 0.6$, where ρ_{in} is the local ion gyroradius). The resulting bubbles contained both strong ion and electron flows. More recently, *Sitnov et al.* [2005, 2007] have described how plasma bubbles would represent a state of reduced cross-tail current associated with the tailward retreat of a small plasmoid or the macroscopic bifurcation of the current.

[6] In the present work we undertake a more general study of kinetic ballooning/interchange modes that can be excited by a tailward gradient in the equatorial magnetic field. We now start from an equilibrium configuration rather than from a dynamically evolving plasma sheet. We find a new class of kinetic ballooning/interchange mode at much shorter wavelength, $k_y\rho_{in} \sim 6$. This new mode is driven by an inverse ion Landau damping process, but the ions remain essentially passive and the currents associated with the magnetic field perturbation are primarily Hall currents associated with the electrons. The mode evolves to form narrow (~500–700 km) magnetic bubbles of enhanced field and reduced density which propagate earthward at speeds of 300–400 km/s. The bubbles act to return flux toward the Earth, but since they are so narrow it requires multiple cycles to fill in the B_z minimum.

[7] The outline of the paper is as follows. Section 2 describes the particle-in-cell simulation model and initial equilibrium configuration. Section 3 presents the simulation results that establish the properties of the magnetic bubbles. A kinetic treatment of the linear properties of the mode is given in section 4; this analysis leads to an identification of the mode as a low-frequency extension of the lower hybrid drift instability. Section 5 contains the summary and discussion.

2. Simulation Model

[8] The simulations to be discussed in this paper employ a 3-D PIC model which retains the full dynamics for both electrons and ions. As described by *Pritchett et al.* [1996, 1997], the electric and magnetic fields are obtained by integrating the time-dependent Maxwell equations forward in time using an explicit leapfrog scheme, and the relativistic particle equations of motion are likewise integrated in time using a leapfrog scheme. A Poisson correction is applied to the electric field to ensure that the current continuity equation remains valid for the charge and current densities interpolated onto the spatial grid [*Pritchett*, 2000]. The spatial storage of the **E** and **B** fields is based on a fully staggered grid system [*Yee*, 1966] in which the components of **E** are defined at midpoints of the cell edges, while the components of **B** are defined at the midpoints of the cell surfaces.

[9] The initial current sheet equilibrium is taken to be of the generalized Harris type [*Schindler*, 1972; *Birn et al.*, 1975; *Lembège and Pellat*, 1982] with isotropic pressure and in which the particle distributions consist of drifting Maxwellians in y. The initial magnetic fields are obtained from the vector potential $A_{0y}(x, z)$ given by

$$A_{0y}(x,z) = B_0 L \ln\{\cosh[F(x)(z/L)]/F(x)\}. \tag{1}$$

Here, $F(x)$ is a slowly varying but otherwise arbitrary function. If $F(x) \equiv 1$, then the solution reduces to the well-known *Harris* [1962] neutral sheet solution. For a nonconstant $F(x)$, there is a finite B_z field which at the center of the sheet ($z = 0$) has the form

$$B_{0z}(x,0) = -B_0 L F'(x)/F(x). \tag{2}$$

[10] For the present investigation, we choose the equatorial field profile to have a minimum similar to that considered previously in 2-D studies by *Pritchett and Büchner* [1995],

$$\begin{aligned} B_{0z}(x,0) &= \epsilon_{\min} + \epsilon_1(1 - x/x_1), \qquad 0 \le x \le x_1 \\ &= \epsilon_{\min}, \qquad x_1 \le x \le x_2 \\ &= \epsilon_{\min} + \epsilon_2[(x - x_2)/(x_3 - x_2)], \qquad x_2 \le x \le x_3, \\ &= \epsilon_{\min} + \epsilon_2, \qquad x_3 \le x \le x_4. \end{aligned} \tag{3}$$

This functional form is illustrated in Figure 1. An initial run in which the B_z profile was taken to be symmetric with respect to

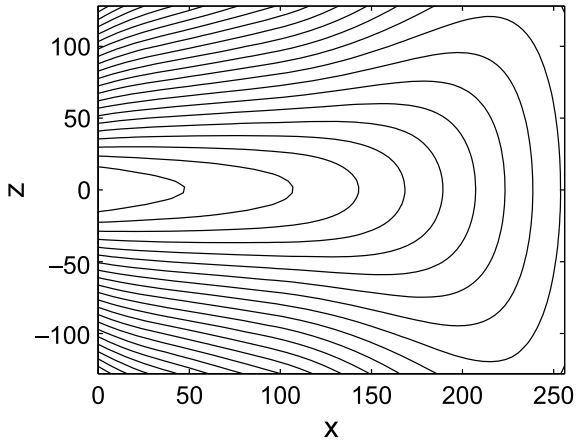

Figure 2. Initial equilibrium field lines in the x, z plane.

the center of the x range revealed that interchange modes developed only in the region with a tailward gradient in B_z. Thus the run to be discussed in this paper uses an asymmetric profile which increases the length of the tailward gradient region at the expense of the (quiet) earthward gradient region. From (2) one then readily obtains

$$\begin{aligned} F(x) &= \exp\{L^{-1}[-\epsilon_{\min}(x-x_1)+\epsilon_1(x-x_1)^2/2x_1]\}, \\ &\quad 0 \le x \le x_1 \\ &= \exp\{L^{-1}[-\epsilon_{\min}(x-x_1)]\}, \qquad x_1 \le x \le x_2 \\ &= \exp\{L^{-1}[-\epsilon_{\min}(x-x_1)-\epsilon_2(x-x_2)^2/2(x_3-x_2)]\}, \\ &\quad x_2 \le x \le x_3 \\ &= \exp\{L^{-1}[-\epsilon_{\min}(x-x_1)-(\epsilon_2/2)(2x-x_2-x_3)]\}, \\ &\quad x_3 \le x \le x_4. \end{aligned} \tag{4}$$

The normalization has been chosen so that $F(x_1) = 1$. The corresponding density distribution is given by

$$n(x,z) = n_0 F^2(x)\mathrm{sech}^2[F(x)(z/L)]. \tag{5}$$

[11] The basic configuration to be studied has a simulation grid $N_x \times N_y \times N_z = 256 \times 512 \times 256$. The ion to electron mass ratio is taken to be $m_i/m_e = 64$, and the temperature ratio is $T_i/T_e = 1$. The ion gyroradius ρ_{i0} in the B_0 field is 16Δ, where Δ is the (uniform) grid spacing, and the characteristic sheet half-thickness is $L/\rho_{i0} = 1.6$. The electron plasma frequency/gyrofrequency ratio based on n_0 is $\omega_{pe}/\Omega_{e0} = 2$, and the electron Debye length is $\lambda_{De} = \Delta$. The profile parameters in the form (3) are $\epsilon_{\min} = 0.10$, $\epsilon_1 = 0.10$, $\epsilon_2 = 0.30$, $x_1 = 32\Delta$, $x_2 = 96\Delta$, and $x_3 = 224\Delta$. The resulting equatorial profiles $B_{0z}(x, 0)$ and $n(x, 0)$ are shown in Figure 1, and the corresponding magnetic field lines in the x, z plane are shown in Figure 2. The local ion gyroradius at the center of the tailward gradient region ($B_z = 0.25\ B_0$) is then $\rho_{in} = 64\Delta$. A typical value of ρ_{in} in the plasma sheet is ~2000 km. The total number of particles in the simulation is 864 million, which corresponds to a reference density n_0 of 106 particles per cell per species.

[12] An important parameter for characterizing the nature of the particle orbits in the initial current sheet equilibrium is the stochasticity parameter κ_j [*Büchner and Zelenyi*, 1987],

$$\kappa_j = (B_{0z}/FB_0)(L^*/\rho_{j0})^{1/2}, \tag{6}$$

where $L^* = L/F(x)$ is the effective half-thickness of the current sheet and j indicates the particle species. For the ions, $\kappa_i < 1$ throughout most of the x range of the simulation, and thus the ion orbits are stochastic. For the electrons, however, κ_e increases through unity at $x \approx 120$, and $\kappa_e \approx 2.5$ at the midpoint of the magnetic field tailward gradient region. Thus on the rightmost portion of this gradient region the electron orbits are adiabatic. In this adiabatic region the plasma beta decreases from of the order of 4 down to a few tenths.

[13] The simulation employs "closed" boundary conditions at the x boundaries [*Pritchett and Coroniti*, 1998]. No magnetic flux is allowed to cross these boundaries, corresponding to the condition $\delta E_y = 0$, and particles that cross the boundary are reinserted back into the system in the opposite half z plane with $v_x = -v_x$ and $v_z = -v_z$ [*Pritchett et al.*, 1991]. In addition, the perturbed field δE_z is assumed to vanish at these boundaries. At the z boundaries, conducting conditions are assumed, and the occasional particle striking such a boundary is reintroduced in the opposite half z plane with $v_x = -v_x$ and $v_z = v_z$. Periodicity in the y direction is assumed for both the particles and fields.

3. Simulation Results

[14] The simulations are performed as a pure initial-value calculation starting from the equilibrium configuration illustrated in Figures 1 and 2. There is no external convection electric field imposed on the system, and the ballooning/interchange modes develop from the initial noise in the system without an explicit perturbation. Figure 3 shows the structure in the equatorial plane at time $\Omega_{i0}t = 37.5$ of the electrostatic potential ϕ (Figure 3a) and the electric field E_y (Figure 3b). Complex, multimode, relatively high k_y wave number structures have developed for both ϕ and E_y in roughly the tailward half of the initial tailward gradient B_z profile. This is the region where the electron orbits are adiabatic. The dominant mode numbers are 8 and 9, although appreciable amplitudes extend from modes 6 through 11. Mode 8 corresponds to $k_y\rho_{in} = 6.3$, and thus the dominant wavelength is $\approx\rho_{in}$, the local ion gyroradius. The longer wavelength modes grow only at later times, and it is unclear whether this represents a true linear growth or is the result of nonlinear mode-mode coupling. The linear growth rate for the development of the dominant modes is $\gamma/\Omega_{i0} \approx 0.13$, and the real frequency is $\omega_r/\Omega_{i0} \approx -0.2$, corresponding to propagation in the direction of the ion drift. The corresponding phase velocity is $\omega_r/k_y \approx 0.2v_{di}$, where $v_{di} = -0.62v_{Ti}$ is the initial ion cross-tail drift. The spatial development of the modes appears to be halted by the short plateau in the B_z profile existing for $224 \le x/\Delta \le 256$. In an earlier run without this plateau in which the B_z gradient continued up to the tailward boundary, the structure of the modes continued to the boundary as well, resulting in increased sensitivity to the boundary conditions. A detailed analysis of the properties of these modes is given in section 4.

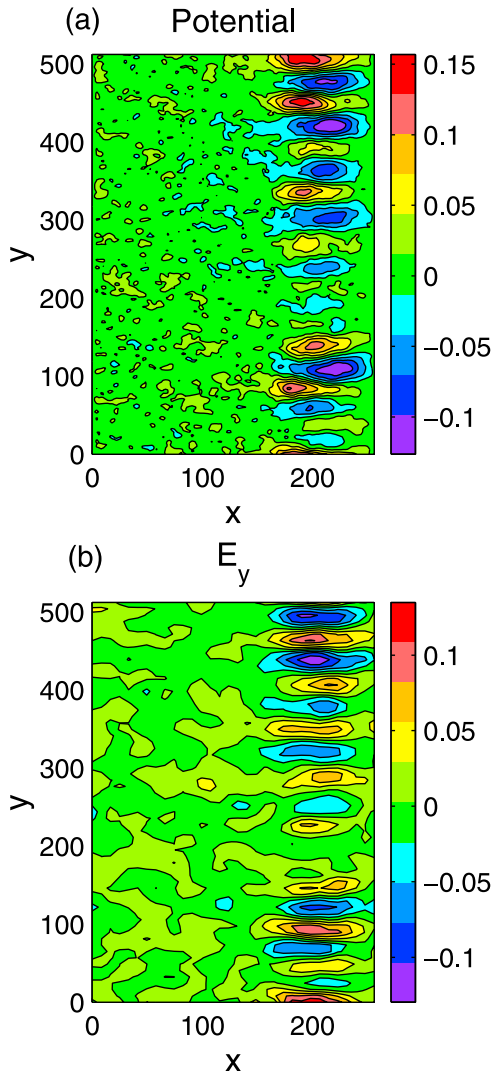

Figure 3. Structure of the ballooning/interchange instability in the equatorial plane at time $\Omega_{i0}t = 37.5$ as manifested in (a) the electrostatic potential $e\phi/(T_i + T_e)$ and (b) the electric field cE_y/v_AB_0.

[15] Figure 4 shows the x, z meridian plane structure of E_y at two different values of y at $\Omega_{i0}t = 37.5$; these two cuts correspond to a local maximum and minimum of the equatorial E_y. Superimposed in white are the magnetic field lines. The maximum E_y field strength occurs for $z = 0$, and the amplitude decays relatively slowly along a field line until it is forced to vanish at the inner boundary ($x = 0$) by the imposed "closed" boundary condition. Such a field structure along the flux tube is characteristic of a classic ballooning mode, but it is unclear from the simulation alone whether this "closed" condition plays any essential role in determining the growth or properties of the relatively localized mode in the plasma sheet. Again, it is apparent that the earthward portion of the tailward B_z gradient does not support the growth of the modes. The E_y (and also ϕ) mode structure is clearly symmetric with respect to $z = 0$. The accompanying perturbation in B_z (maximum value of $\approx 0.03B_0$ at this time) is also symmetric in z, while that in B_x is antisymmetric. The B_y perturbation is very small. The mode structure is thus dominated by $\delta\phi$ and $\delta B_{\|}$.

[16] As the modes continue to grow, the equatorial plane structure begins to exhibit the classic bubble or finger features characteristic of a Rayleigh-Taylor instability. Figure 5 shows a sequence of plots of B_z in the equatorial plane at times equally spaced between $\Omega_{i0}t = 42$ and $\Omega_{i0}t = 66$. By $\Omega_{i0}t = 52$ (Figure 5c), the regions of enhanced B_z have penetrated across almost all of the initial tailward gradient B_z region. The growth of this bubble structure is associated with a strong perturbation of the electron flow velocity as shown in Figure 6. The initial dawnward flow is distorted into a series of swirls or vortices that provide the (Hall) currents associated with the magnetic field perturbations. As shown in Figure 7, the perturbations in the electron flow are as large as 1.0–1.5 v_{Ti}. In contrast, the perturbations in the ion flow are much smaller. Thus the ions are basically unaffected by the modes.

[17] Unlike the case of interchange modes in MHD, there is a substantial perturbation resulting from the finite $E_{\|}$ field.

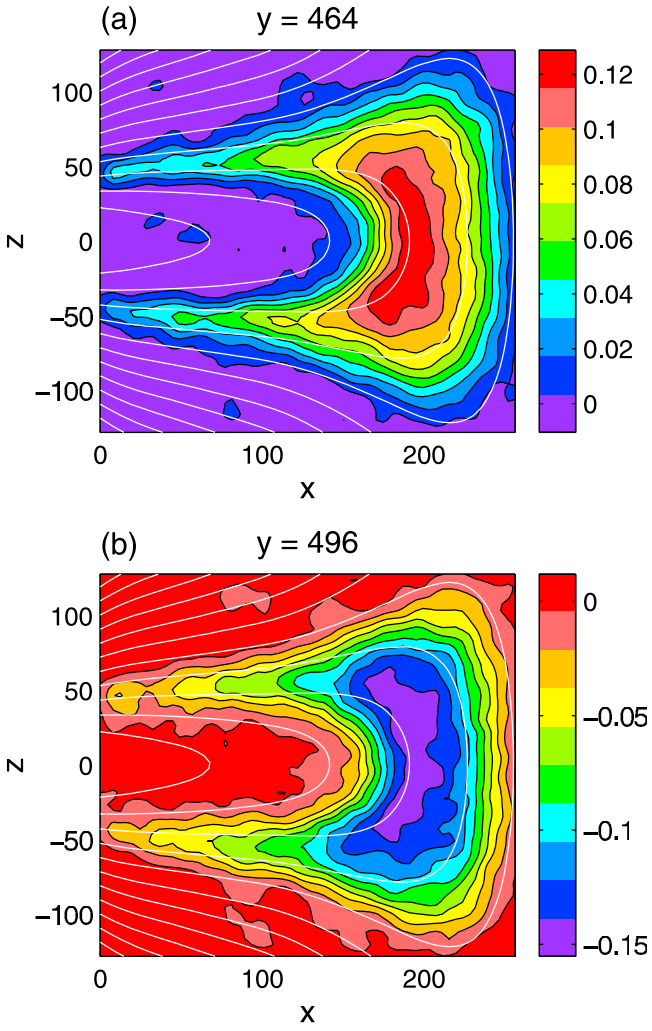

Figure 4. Structure of the ballooning/interchange instability in an x, z meridian plane at time $\Omega_{i0}t = 37.5$ as manifested in the electric field cE_y/v_AB_0 at values of (a) $y = 464$ and (b) $y = 496$. Superimposed in white are the projections of the magnetic field lines in these planes.

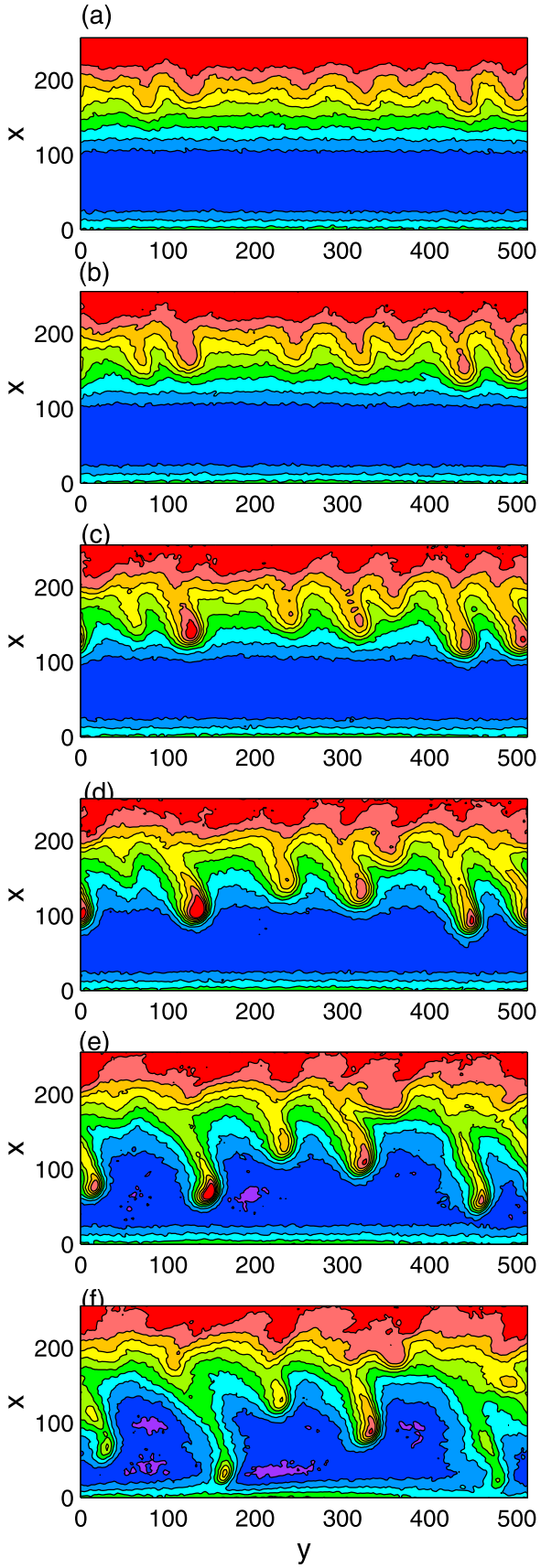

Figure 8 shows the parallel electron velocity flow in two x, z meridian planes at time $\Omega_{i0}t = 47$. Particularly noteworthy features of this flow are that it reverses sign at high values of z and that the maximum $|v_{||}|$ occurs on field lines that pass well outside the region of maximum E_y in the equatorial plane (cf. Figure 4).

[18] At later times the flux fingers narrow in cross tail extent (to between 0.3–0.5 ρ_{in} or ~500–700 km) and reach the earthward edge of the simulation (Figure 5f). The inward flow speed of one of the bubbles is about 0.3–0.4 v_{Ti}. Figure 9 shows a series of x profiles through the bubble at $y = 332$ in Figure 5f. The most prominent feature is the sharp increase in B_z from about $0.1B_0$ to $0.4B_0$ at the head of the bubble. This "local dipolarization" is accompanied by a fairly sharp drop in density (by about a factor of two) and almost stagnant ion flow ($|v_{xi}| < 0.02v_{Ti}$). While the magnetic field dipolarization is very dramatic, it only occurs over a region of some 500–700 km across the tail. Thus one needs to exercise caution in assessing the global significance of single spacecraft observations of magnetic field dipolarization.

[19] The magnetic bubbles clearly act to return flux toward the Earth. The dashed line in Figure 9a shows the initial B_z profile. It is clear that the B_z field for $x \gtrsim 200$ and $y = 332$ has been reduced only slightly by the development of the bubble. Thus the bubbles must draw flux from the sides, as is also suggested by the scalloped nature of the high B_z region in Figure 5b. Since there is still a considerable region of high B_z at the tailward boundary of the simulation, it is quite possible that a second wave of fingers could be excited. Thus it is possible that a succession of bubbles would be needed to completely fill in the initial B_z minimum. To check this hypothesis, one needs to increase the x dimension of the simulation so that the bubbles can be followed for a longer time.

4. Mode Identification

[20] The dominant unstable mode has a real frequency $\omega_r/\Omega_{i0} = -0.21$, a growth rate $\gamma/\Omega_{i0} = 0.13$, wave number $k_y\rho_{i0} = 1.57$, and a phase speed of $\omega_r/k_y v_{Ti} = -0.125$ in the direction of the equilibrium ion drift velocity. In this section, we show that these parameters satisfy a linear dispersion relation that is the generalization to curved magnetic field geometry of the interchange (Rayleigh-Taylor) or lower hybrid drift (LHD) modes that were investigated in linear magnetic geometry by *Huba et al.* [1987] and *Winske* [1996]. From the simulation results, the dominant polarizations of the mode are the perturbed electrostatic potential $\delta\phi$ and the perturbed parallel component of the magnetic field $\delta B_{||}$, the dominant polarizations of the LHD in straight magnetic geometry. We focus on the mode structure near $x = 192\Delta$, $y = 464\Delta$ at time $\Omega_{i0}t = 37$ where the equatorial magnetic field strength is $B_{0z} = 0.338B_0$, and the equilibrium vector potential has the value $A_{0y}/LB_0 = 1.09$. We use the simulation results to model the dependence of $\delta\phi(l)$ and

Figure 5. Development of the bubble structure of the ballooning/interchange instability in the equatorial plane as manifested in the magnetic field B_z/B_0 at times equally spaced between (a) $\Omega_{i0}t = 42$ and (f) $\Omega_{i0}t = 66$. The color scale runs from a maximum of 0.42 to a minimum of 0.05.

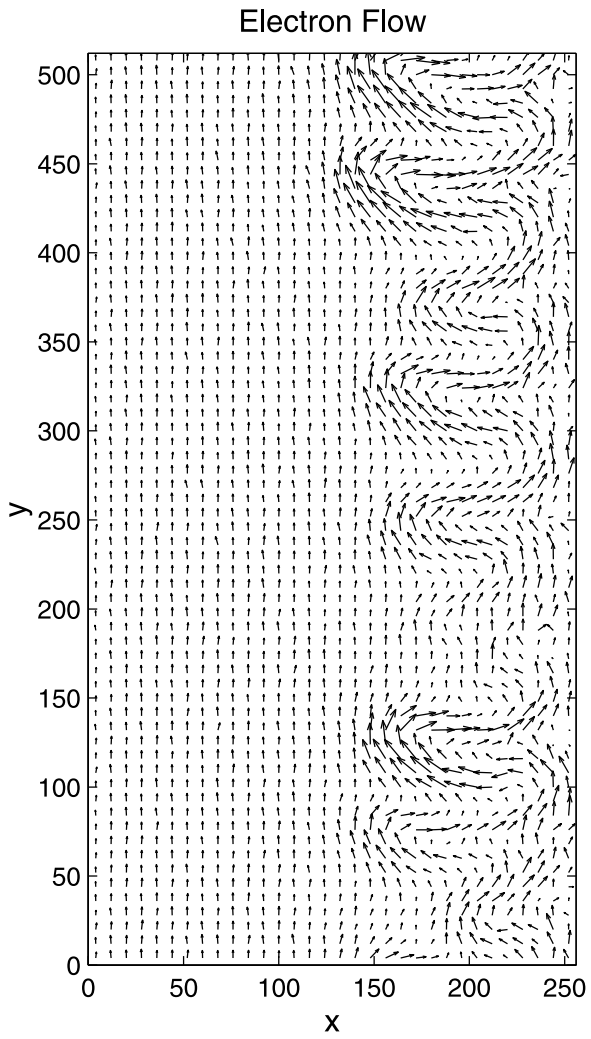

Figure 6. Vector field structure in the equatorial plane ($z = 0$) at time $\Omega_{i0}t = 47$ of the electron flow velocity.

$\delta B_{\parallel}(l)$ along the equilibrium field lines and evaluate the local ion (δn_i) and electron (δn_e) density perturbations at the midplane ($l = 0$) of the simulation. The local dispersion relation follows by averaging (denoted by $\langle\ \rangle$) the perturbed densities over the flux tube volume $V = \int dl/B$ (usually denoted as $V' = \partial V/\partial\Psi = \int dl/B$, with Ψ being the equilibrium vector potential or flux function coordinate), and setting $\langle \delta n_i \rangle = \langle \delta n_e \rangle$.

4.1. Perturbed Ion Density

[21] In evaluating the perturbed ion distribution function, we assume that the ion orbits are unmagnetized even though the formal validity for this assumption $\gamma/\Omega_i > 1$ is not satisfied at the midplane. The ion orbits are stochastic ($\kappa_i \ll 1$), thus destroying the periodic gyromotion. Furthermore, the unstable mode is localized in both the x and z directions to scales of order ρ_{in}; thus the ions transit through the wave essentially in straight lines. (A very involved model of the ion orbits that included the spatial localization of the eigenfunction and quasi-gyromotion in the normal magnetic field yielded a result that was nearly identical to the straight line orbit approximation.) Since the ions primarily only respond to the electrostatic potential perturbation, the local perturbed ion density is given by the classic result

$$\delta n_i/n_L = [Z'(s)/2]e\delta\phi/T = -[1 + sZ(s)]e\delta\phi/T,$$
$$s = (\omega - k_y v_{di})/k_y v_{Ti} \tag{7}$$

where $Z(s)$ is the plasma dispersion function, and $n_L = 0.1n_0$ is the local plasma density at $x = 192\Delta$. For the parameters of the unstable mode, $s = 0.49 + 0.083i$, and $\delta n_i/n_L = -[0.532 + 0.577i]\ e\delta\phi/T$. However, the phase relation between δn_i and $\delta\phi$ implied by this result is not in accord with the measured phase relation in the simulation.

[22] The first term ($-e\delta\phi/T$) in (7) is the local Boltzmann response. However, the $sZ(s)$ term originates from an orbit integral over the past history of an ion's interaction with the wave, and the orbital motion averages over the spatial decrease of $\delta\phi(x,z)$ away from the maximum amplitude location ($x = 192\Delta$, $z = 0$). If we model the x dependence of $\delta\phi$ as $\delta\phi_0 \exp[-(x - 192)^2/\delta^2]$ with $\delta = 26.7\Delta$ as measured from the simulation and use the local gyroradius $\rho_{in} = 47.3\Delta$ as the effective orbital excursion about $x = 192\Delta$, we find the effective orbital spatial average of $\delta\phi$ is $\langle \delta\phi/\delta\phi_0 \rangle_x = (\sqrt{\pi}/2)\ (\delta/\rho_{in})\mathrm{erf}(\rho_{in}/\delta) \approx 1/2$. We can also use the simulation results to model the spatial decrease of $\delta\phi(l)$ along the field lines as $\delta\phi_0 \exp[-3.94(\xi_0 - \xi)^2]$, where $\xi \equiv \epsilon x/L$ and $\xi_0 = 0.625$ corresponds to $x = 192\Delta$. The exponential function models the length l along a field line for the flux surface $A_{0y}/LB_0 = 1.09$. Again, we find that $\langle \delta\phi/\delta\phi_0 \rangle_l \approx 1/2$. Thus the reduction of the ion's response due to the orbit averaging over the spatial decrease of $\delta\phi$ can be roughly modeled by multiplying the $sZ(s)$ term by 0.5.

[23] Since the electron orbits average the interaction with the wavefields over the volume of the flux tube, to obtain

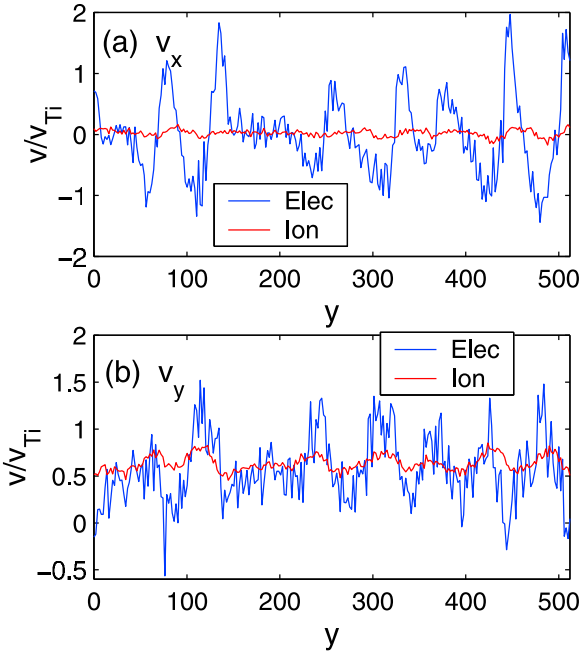

Figure 7. Velocity flow profiles as a function of y at time $\Omega_{i0}t = 47$ at $x = 170$ and $z = 0$ for the electrons (blue curves) and the ions (red curves) for (a) the v_x component and (b) the v_y component.

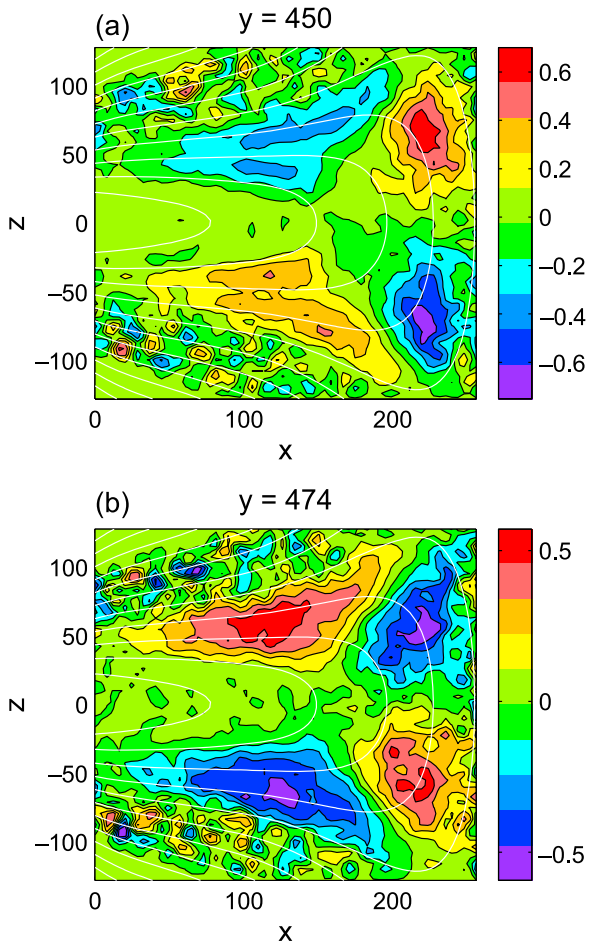

Figure 8. Structure of the parallel (to the magnetic field) electron velocity flow $v_{e\|}/v_{Ti}$ in an x, z meridian plane at time $\Omega_{i0}t = 47$ at values of (a) $y = 450$ and (b) $y = 474$. Superimposed in white are the projections of the magnetic field lines in these planes.

the dispersion relation, we average the bare Boltzmann term in (7) by taking $\delta\phi = \delta\phi_0 h(l)$, modeling the field line variation $h(l)$ using the simulation results (see (15) below), and then performing the flux tube average to obtain $\langle\delta\phi\rangle = \delta\phi_0\langle h(l)\rangle \approx 0.75\delta\phi_0$. The $sZ(s)$ term is assumed to already be averaged when reduced to one-half of its bare value. With these spatial averaging operations, the flux tube-averaged perturbed ion density becomes

$$\langle\delta n_i/n_L\rangle = -[0.75 + sZ(s)/2]e\delta\phi_0/T = -[0.515 + 0.289i]e\delta\phi_0/T. \quad (8)$$

Clearly, orbit averaging has significantly reduced the imaginary part of $\delta n_i/n_L$. As a check of (8), we measured the magnitude and phase shift relations between δn_i and $\delta\phi$ in the simulation region between $y = 400\Delta$ and 500Δ. The relative peak amplitudes and the spatial phase shift between the peaks of $\delta y = 4.9\Delta$ or $k_y\delta y = 0.48$ agree with the values shown in (8) and disagree with the values obtained from (7).

4.2. Perturbed Electron Density

[24] In the $\partial B_z/\partial x > 0$ region, the electron orbits are adiabatic (the first invariant $\mu = v_\perp^2/B$ is conserved) and described by guiding center theory. However, $|\omega\tau_B|$ and $|\omega_D\tau_B|$ (defined below) are of order unity for some values of μ and E (energy). Thus the conventional expansion where the wave and drift frequencies are small compared with the bounce frequency is not applicable, and the full kinetic response including bounce and drift resonance interactions must be retained. Fortunately, $k_y\rho_e \ll 1$, and electron Larmor radius corrections can be neglected.

[25] After averaging over the rapid electron gyrofrequency timescale, the perturbed electron distribution function for the assumed dominant $\delta\phi$ and $\delta B_\|$ polarizations is

$$\delta f_e = -q\delta\phi/T + f_{1e}, \quad (9)$$

$$f_{1e} = -iq[(\omega - \omega_*)/T]f_0 \exp(ik_x x_0)\int_{-\infty}^{0} dt \exp[-i\omega t + ik_y y_0(t)] \times [\delta\phi J_0 + (v_\perp J_1/k_\perp c)\delta B_\|], \quad (10)$$

where $q = -e$, f_0 is the equilibrium Maxwellian distribution function, $\omega_* = k_y u_e$ with $u_e = -cT/e\partial\ \ln(n_0)/\partial\Psi = 2cT/eB_0L$ being the electron diamagnetic drift speed, $t = 0$ is the present time, $x_0 = x(0) + v_\perp/\Omega_e \sin\theta_0$, $y_0 = y(0) - v_\perp/\Omega_e\cos\theta_0$, θ_0 is the

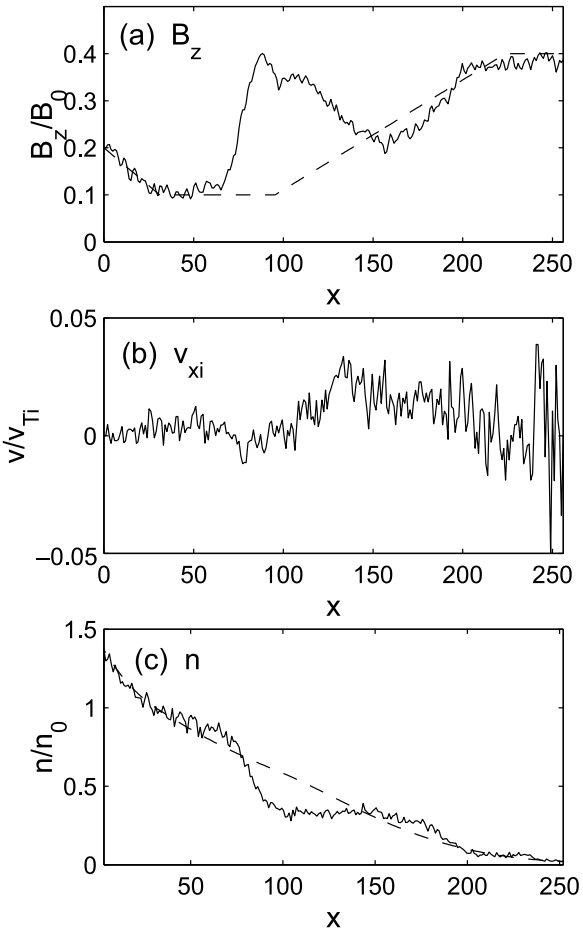

Figure 9. Profiles as a function of x through an interchange bubble at $y = 332$ and $z = 0$ at time $\Omega_{i0}t = 66$: (a) the magnetic field B_z, (b) the ion velocity v_{ix}, and (c) the density n. The dashed lines in Figures 9a and 9c represent the initial equilibrium profiles.

Larmor phase, $y_0(t) = y_0(0) + \int_0^t v_D(t')dt'$, $v_D(t)$ is the guiding center drift speed in the y direction, $k_\perp$ is the perpendicular wave number, and $J_n(k_\perp v_\perp/\Omega_e)$ is a Bessel function.

[26] Expanding J_n to lowest order, converting the orbit integral into summations over past bounce periods, summing the result, and integrating over velocity space yields the perturbed electron density

$$\delta n_e/n_L = e\delta\phi/T + n_{1e}/n_L, \tag{11}$$

$$n_{1e}/n_L = [ie(\omega-\omega_*)/\sqrt{\pi}T_e^{5/2}]\int_0^\infty dE\exp(-E/T)\int_0^{E/B} \cdot [Bd\mu/(E-\mu B)^{1/2}]\hat{O}(\overline{\omega_D}\tau_B)[\overline{\delta\phi} - (\mu/e)\overline{\delta B_\parallel}], \tag{12}$$

where the overbar denotes the bounce average $(1/\tau_B)\oint dl/|v_\parallel|$, $\omega_D = k_y v_D$, and the time operator

$$\hat{O}(\overline{\omega_D}\tau_B) = \frac{\exp[(3/4)i(\omega-\overline{\omega_D})\tau_B]\cos^2[(\omega-\overline{\omega_D})\tau_B/4]}{1-\exp[i(\omega-\overline{\omega_D})\tau_B]} + \frac{1}{4}\exp[i(\omega-\overline{\omega_D})\tau_B/4]. \tag{13}$$

The Ampere equation $ik_y\delta B_\parallel = (4\pi/c)\delta J_\Psi = -4\pi e/c\int v_\perp\cos\theta\, f_{1e}d^3v$ yields

$$\delta B_\parallel = -[ie(\omega-\omega_*)/\sqrt{\pi}T_e^{5/2}]\int_0^\infty dE\exp(-E/T)\int_0^{E/B} \cdot [\mu B d\mu/(E-\mu B)^{1/2}]\hat{O}(\overline{\omega_D}\tau_B)[\overline{\delta\phi} - \mu\overline{\delta B}_\parallel/e]. \tag{14}$$

The only approximation that has been made in obtaining the above results is to bound the value of one phase integral that appears in the time operator $\hat{O}$ by assuming

$$\int_0^l (dl/|v_\parallel|)[\omega-\omega_D] < \int_0^{lm}(dl/|v_\parallel|)[\omega-\omega_D] = (1/4)[(\omega-\overline{\omega_D})\tau_B],$$

where lm is the mirror point which allowed the orbit integral to become a nonlocal function of the bounce-averaged ω_D. The $\hat{O}$ operator contains all of the bounce and drift resonant contributions. If we expand for the usual ordering $(\omega-\omega_D)\tau_B \ll 1$, then (11) and (14) reduce to the results of *Hurricane et al.* [1995] (and many others).

[27] We assume that both the perturbed electrostatic potential and parallel magnetic field vary along the equilibrium field lines as $\delta\phi = \delta\phi_0 h(l)$ and $\delta B_\parallel = \delta B_{\parallel 0} h(l)$. The parallel eigenfunction $h(l)$ was determined by fitting the variation of $\delta\phi(l)$ from the simulation along the field line that passes through the maximum potential and crosses $z = 0$ at $x = 192\Delta$. Letting $x' = x + 32\Delta$ (so that $x' = 0$ corresponds to the start of the constant B_z region), we found that

$$\begin{aligned} h(l) &= \exp[-(160 - x'/\Delta)^2/65], \qquad 110 \le x'/\Delta \le 160 \\ &= 0.56\ \mathrm{sech}[(110 - x'/\Delta)/54], \qquad 0 \le x'/\Delta \le 110 \end{aligned} \tag{15}$$

gave a reasonable fit to the simulation results. Performing the bounce average of $h(l)$ in (11) and (14) converts $h(l)$ into $h(\mu, E)$.

[28] We now average δn_e and $\delta B_\parallel$ over the flux tube volume using the relation [*Hurricane et al.*, 1995]

$$(1/V)\int dl/B\int Bd\mu dE/|v_\parallel| = (1/2V)\int dEd\mu\oint dl/|v_\parallel|.$$

The integral over $d\mu$ can be converted into an integral over the magnetic field strength at the electron mirror point B_m ($d\mu = -(E/B_0)db/b^2$; $b = B_m/B_0$), thereby decoupling the $d\mu$ and dE integrals. The resulting multiple integrals were then evaluated numerically using the numerically calculated bounce averages of $\delta\phi$ and $\delta B_\parallel$ as functions of B_m and E. Equations (11) and (14) have the final form

$$\langle\delta n_e\rangle/n_L = [\langle h\rangle + I_\phi^n]e\delta\phi_0/T + I_B^n\delta B_{\parallel 0}/B_0, \tag{16}$$

$$\langle h\rangle\delta B_{\parallel 0}/B_0 = I_\phi^B e\delta\phi_0/T + I_B^B\delta B_{\parallel 0}/B_0. \tag{17}$$

The coefficients I_i^j are just the velocity space integrals obtained by first integrating over dE at fixed B_m and then integrating over B_m from $0.3 \le B_m/B_0 \le 1.0$. In the equilibrium, the magnetic field strength actually decreases from the midplane value $B_n/B_0 = 0.338$ to $B/B_0 = 0.3$ as l increases from zero and then rises to B_0 near the edge of the simulation region. Thus some electrons can be trapped between mirror points on each side of the midplane. These high pitch angle electrons have drift speeds $v_D < 0$ and can therefore be in drift resonance ($\omega_r - \omega_D = 0$) for real frequency $\omega_r < 0$.

[29] If we limit the range of the integral over $0.3 < B_m/B_0 \le 1$, the values of the above coefficients for the simulation wave frequency and wave number are

$$I_\phi^n = -1.71 - 0.67i \qquad I_\phi^B = 0.1 + 0.78i$$

$$I_B^n = 5.0 + 3.0i \qquad I_B^B = -0.595 - 0.664i$$

Eliminating $\delta B_\parallel$ yields the relation between δn_e and $\delta\phi$

$$\begin{aligned} \langle\delta n_e\rangle/n_L &= [\langle h\rangle + I_\phi^n + I_B^n I_\phi^B/(\langle h\rangle - I_B^B)]e\delta\phi_0/T \\ &= [-0.59 - 0.336i]e\delta\phi/T. \end{aligned} \tag{18}$$

Thus for the observed simulation results, the calculated perturbed electron (18) and ion (8) flux tube averaged densities are in reasonable agreement, especially considering the rather approximate modeling of the spatial orbit averaging in the calculation of the ion response.

[30] The ratio of $\delta B_\parallel$ to $\delta\phi$ is calculated to be

$$\frac{\delta B_\parallel/B_0}{e\delta\phi/T} = 0.084 + 0.0167i \equiv r\exp(i\theta),\ r = 0.086,\ \theta = 0.196\ \mathrm{rad}.$$

In the simulation region near $y = 400\Delta$, the measured amplitude ratio is about 0.08 and the peaks of $\delta B_\parallel$ and $\delta\phi$ are separated by $\delta y = 1.9\Delta$ for a phase shift of $k_y\delta y = 0.19$ rad.

[31] The calculated kinetic electron and ion responses agree with the simulation observed relationships between the wave polarizations, and they combine to yield a dispersion relation that is satisfied by the observed wave frequency and growth rate for the measured dominant wave number. Thus the broad agreement between theory and simulation argues that the above calculation has captured the basic dynamics of the unstable modes.

[32] However, one uncertainty about the calculation remains. We cut off the integral over B_m/B_0 at unity, whereas, in principle, small pitch angle electrons would extend this ratio to infinity. The maximum field strength at the edge of the simulation ($x = 0$) reaches $B = 1.17B_0$. If we just extend

the range of the B_m/B_0 integration up to 1.2, the values of the I_i^j shift sufficiently that the agreement between the real parts of $\langle \delta n_i \rangle$ and $\langle \delta n_e \rangle$ is significantly weakened; the calculated phase shift between $\delta B_\parallel$ and $\delta\phi$ still agrees with the simulation results. If the B_m integration is extended to $B_m/B_0 = 4.0$, the real part of δn_e disagrees with the real part of δn_i by almost a factor of two; the calculated phase shift between $\delta B_\parallel$ and $\delta\phi$ now disagrees but only by 10%. These numerical results seem to indicate that only the relatively deeply trapped ($B_m/B_0 \le 1$) electrons significantly contribute to the mode dynamics. Electrons with smaller equatorial pitch angles reflect near the $x = 0$ edge of the simulation box, or, being in the loss cone, are reflected from the simulation wall and reintroduced in the opposite half z plane. Our past experience with these complex spatially inhomogeneous simulations is that electrostatic sheaths containing intense spatially and temporally varying fluctuating electric fields can develop near the edge of the simulation box, especially on the earthward side. Perhaps these strong fields scatter the electrons that reach the sheath region and thereby destroy the coherent response of these small pitch angle electrons to fields of the unstable wave mode.

4.3. Mode Identification: Lower Hybrid Drift

[33] The dominant polarizations $\delta\phi$ and $\delta B_\parallel$ observed in the simulation are similar to the polarization of the lower hybrid drift mode in straight magnetic field geometry, which suggests that the ballooning/interchange mode is closely related to the LHD instability. In this section, we demonstrate this relation by deriving the LHD dispersion relation for curved magnetic geometry assuming kinetic ions and fluid electrons.

[34] For the above polarizations (and taking $\delta A_y = \delta A_\parallel = 0$), neglecting the electron inertia ($m_e = 0$), and for isothermal electrons, the electron fluid momentum equation reduces to

$$\delta v_y = -c\delta E_\Psi/B - u_{ye}\delta B/B - (cT/e)(\partial/\partial\Psi)(\delta n_e/n_L), \quad (19)$$

$$\delta v_\Psi = c\delta E_y/B + i(k_y cT/eB)(\delta n_e/n_L), \quad (20)$$

$$\partial/\partial l(\delta n_e/n_L - e\delta\phi/T) = 0. \quad (21)$$

Computing the $\nabla \cdot \delta\mathbf{v}$, the electron continuity equation becomes

$$i(\omega - \omega_D)(\delta n_e/n_L) = i(\omega_* - \omega_D)(e\delta\phi/T) + i(\omega - \omega_*)(\delta B_\parallel/B) + B\frac{\partial}{\partial l}(\delta v_\parallel/B), \quad (22)$$

where $\omega_D = (k_y cT/e)\,(\partial/\partial\Psi)\,(\ln J)$ with J being the magnetic coordinate Jacobian. The Ampere law yields

$$\delta B_\parallel/B = (4\pi n_L T/B^2)(e\delta\phi/T - \delta n_e/n_L) \quad (23)$$

Averaging over the flux tube volume with $\delta v_\parallel = 0$ at the earthward ends of the field lines, noting that $\delta n_e/n_L - e\delta\phi/T = \langle \delta n_e/n_L \rangle - \langle e\delta\phi/T \rangle$, and eliminating $\langle \delta B_\parallel/B \rangle$ from (22) using (23) yields the relation

$$[\omega - \langle\omega_D\rangle + (\omega - \omega_*)\langle\beta_e\rangle/2]\langle\delta n_e/n_L\rangle = [\omega_* - \langle\omega_D\rangle + (\omega - \omega_*)\langle\beta_e\rangle/2]\langle e\delta\phi/T\rangle, \quad (24)$$

where $\langle\beta_e\rangle = \langle 8\pi n_L T/B^2\rangle \approx 0.3$, and $\langle\omega_D\rangle = (k_y cT/e)\,\partial \ln V/\partial\Psi$.

[35] As an aside, the ballooning/interchange and/or LHD instabilities are often analyzed using straight field line geometry but including a gravitational acceleration $\mathbf{g}$ to model magnetic curvature and gradient effects. The gravitational drift velocity $\mathbf{v}_g = (mc/q)\,(\mathbf{g} \times \mathbf{B}/B^2)$ reproduces the guiding center drift velocity if $\mathbf{g} = -(\mu/m)\nabla\mathbf{B} - mv_\parallel^2 B(\hat{\mathbf{s}} \cdot \nabla\hat{\mathbf{s}})$ where $\hat{\mathbf{s}} = \mathbf{B}/B$. In 2-D magnetic geometry only the Ψ component of $\mathbf{g}$ ($g_\Psi = -(\mu B/m)\,\partial B/\partial\Psi + v_\parallel^2 B\partial\ln(JB)/\partial\Psi$) enters. Averaging g_Ψ over an isotropic Maxwellian, we find $g_\Psi = (T/m)\,B\partial\ln(J)/\partial\Psi$, so that the effective drift speed becomes $v_g = (cT/e)\partial\ln(J)/\partial\Psi$. Thus the term $\langle\omega_D\rangle$ in (24) is equivalent to the gravitational acceleration term that appears in the 2-D analyses found in the work of *Huba et al.* [1987] and *Winske* [1996].

[36] For the simulation parameters, $\langle\omega_D\rangle/\Omega_{0i} = 0.365$, $\omega_*/\Omega_{0i} = 1.0$, and $\langle e\delta\phi/T\rangle = \langle h\rangle e\delta\phi_0/T$, (24) yields

$$\langle\delta n_e\rangle/n_L = [-0.417 - 0.102i]e\delta\phi_0/T. \quad (25)$$

Thus for the fluid equations with the LHD polarizations, the relation between the real part of the electron density and the electrostatic potential is in reasonable agreement with the simulation results. Not surprisingly, however, the kinetic drift and bounce resonance contributions significantly alter the imaginary part of the electron's response to $\delta\phi$.

[37] Upon setting $\langle\delta n_e\rangle = \langle\delta n_i\rangle$, the dispersion relation for the LHD mode can be written as

$$\frac{(\omega - \omega_*)}{(\omega - \omega_*)(1 + \langle\beta_e\rangle/2) + \omega_* - \langle\omega_D\rangle} = -2 + \frac{s}{2\langle h\rangle}Z(s) \equiv Q_r + iQ_i. \quad (26)$$

The approximate solution for $|\omega| \ll \omega_*$ is

$$\omega_r \approx \frac{Q_r(\omega_* - \langle\omega_D\rangle)}{Q_r(1 + \langle\beta_e\rangle/2) - 1}, \qquad \gamma \approx \frac{Q_i(\omega_* - \langle\omega_D\rangle)}{[Q_r(1 + \langle\beta_e\rangle/2) - 1]^2}. \quad (27)$$

For the simulation parameters, $Q_r = 1.69$ and $Q_i = 0.385$, (27) yields $\omega_r/\Omega_{0i} = -0.12$ and $\gamma/\Omega_{0i} = 0.256$, which is close to the exact solution to (26). Note that the stability of the LHD mode is determined by the sign of $\omega_* - \langle\omega_D\rangle$ which is proportional to $-(\partial\ln P/\partial\Psi + \partial\ln V/\partial\Psi)$, essentially the classic MHD instability criterion $\gamma V''/V' + P'/P < 0$ of *Bernstein et al.* [1958] (with the MHD conventional notation $V' = \partial V/\partial\Psi = \int dl/B$ and an isothermal ($\gamma = 1$) equation of state).

4.4. Conclusion

[38] The above analysis provides circumstantial evidence, but certainly not definitive proof, that the ballooning/interchange instability observed in the curved magnetic geometry of the simulations is closely related to the lower hybrid drift instability in straight magnetic fields, albeit the low-frequency extension of the LHD. The fluid treatment of the electrons, even in curved field line geometry, however, does not accurately produce the observed simulation results. The kinetic electron bounce and drift resonance effects are clearly important in explaining the simulation results.

5. Summary and Discussion

[39] The present simulations have shown that a plasma sheet equilibrium with a minimum in the magnetic normal

(B_z) component is unstable to a ballooning/interchange-type mode that is localized tailward of the minimum in the positive gradient region of B_z. The mode has a relatively short dawn-dusk wavelength of the order of the ion Larmor radius in the B_z field (~2000 km), has a phase velocity in the direction of and about 1/5 the magnitude of the ion diamagnetic current drift speed, and a real frequency (growth rate) of about 0.6 (0.4) of the midplane ion cyclotron frequency. In its nonlinear evolution, the mode develops Rayleigh-Taylor-type fingers of somewhat reduced cross-tail extent (~500–700 km) that extend through the constant B_z minimum region and into the near-Earth dipole region. The fingers transport magnetic flux toward the Earth. However, within the flux fingers, the earthward ion flow velocity remains low; the flux is redistributed by electron Hall currents that flow around the fingers. Thus this short wavelength ballooning/interchange mode is probably not the origin of the bursty bulk flows (BBFs) that occur on a somewhat larger scale (~several R_E) and transport earthward both plasma and magnetic flux [*Angelopoulos et al.*, 1992].

[40] The present mode is quite different from the kinetic ballooning mode described by *Cheng and Lui* [1998]. This latter mode is believed to be excited near substorm onset in the near-Earth plasma sheet (~8–10R_E) when the plasma beta exceeds 50, the pressure becomes isotropic, and a low-frequency instability with a wave period of ~50–75 s is excited. This mode has $k_\perp \rho_{in} \sim$ O(1), $k_\parallel \ll k_\perp$, and $v_{Te} > \omega/k_\parallel > v_{Ti}$. In contrast, the present mode requires adiabatic electrons, occurs for $\beta \lesssim$ O(1), has $k_\parallel \approx k_\perp$, $v_{Ti} > \omega/k_\perp$, $k_\perp \rho_{in} \sim 6$, and a shorter wave period of ~10 s. This mode is expected to occur in the mid tail (~15–20R_E) and is not expected to be correlated with substorm onset.

[41] The dominant $\delta\phi$ and $\delta B_\parallel$ polarization observed in the simulation suggests that the observed ballooning/interchange mode is related to the lower hybrid drift wave. The LHD mode is not (as is often claimed) a source of anomalous resistance since, in its prototypical straight magnetic field line kinetic-ion, fluid-electron version, the mode does not resonantly transfer momentum between the electron and ion current drifts. The LHD instability is really an interchange mode, with dissipative (Landau resonant) ions and non-dissipative (adiabatic) fluid electrons that nonlinearly spreads the current by interchanging low plasma density (low current carrying) flux tubes with higher-density (higher current carrying) flux tubes. For the magnetically curved geometry of a plasma sheet equilibrium and the particular simulation parameters (especially the high electron-to-ion mass ratio), the electron response to the ballooning/interchange mode involves significant bounce and drift resonant interactions, suggesting that both ion and electron kinetic effects are likely to be important in accurately describing plasma sheet turbulence. Simply stated, the plasma sheet is not a fluid medium, even for electrons.

[42] In the simulation, the ballooning/interchange mode is localized to the tailward B_z gradient region for reasons that are not readily apparent. Within the gradient region, the electrons are well-magnetized ($\kappa_e \approx 3.6$), and their orbits are adiabatic; thus the electron's response to the mode's electrostatic potential is a fluid-like $\mathbf{E} \times \mathbf{B}$ drift that creates the Hall current needed to self-consistently produce the mode's $\delta B_\parallel$ polarization. In the near-Earth minimum and constant B_z region, the electron orbits are stochastic ($\kappa_e \approx 0.36$). From the analysis of *Hurricane et al.* [1995], the principal change in the electron's kinetic response to the wave is to replace the adiabatic orbit bounce-averaged fields ($\delta\phi$ and $\delta B_\parallel$) and drift frequency (ω_D) with stochastic μ-averaged (pitch angle) and flux tube volume averaged quantities; in effect, the stochastic electron response becomes isothermal. (In an early attempt to explain the simulation results, we computed the electron response using the *Hurricane et al.* [1995] stochastic orbit formalism, but the results did not agree numerically with the ion density perturbation.) We did simulate the Lembège and Pellat equilibrium with a constant, small normal magnetic field [*Lembège and Pellat*, 1982] and moderately adiabatic electrons and found that the system was weakly unstable [*Pritchett*, 2002], in agreement with a prediction based on ideal MHD [*Hurricane et al.*, 1996]. Thus the localization of the ballooning/interchange mode to the B_z gradient region may just indicate that the instability is stronger when the electrons are adiabatic or well-magnetized. Clearly, a full dispersion relation analysis is needed in order to explore the dependence of the ballooning/interchange mode's frequency and growth rate on the parameters of the equilibrium and to clarify the possible role of the vanishing E_y boundary condition in enabling the growth of the mode. This would help to establish whether the ballooning or interchange character of the mode predominates.

[43] Finally, *Saito et al.* [2008a, 2008b] have presented evidence for the growth of the MHD interchange mode in the high-β ($\beta > 20$–70) current disruption region just before the onset of substorm breakup. The MHD mode had an oscillation frequency of 0.01–0.02 Hz in the spacecraft frame, which was interpreted as being a zero frequency wave in the ion rest frame, and a dawn-dusk wavelength of 2000–5000 km. Since the simulated ballooning/interchange mode would have a higher frequency (0.06 Hz) and a somewhat shorter wavelength (1000–2000 km), the relationship between *Saito et al.*'s [2008a, 2008b] observations and the simulation results is not clear.

[44] In conclusion, the simulation investigation suggests that the plasma sheet with a finite magnetic normal component and a positive earthward gradient in flux tube content ($\gamma \sim -\partial \ln (nV)/\partial \ln(\Psi)$, equation (27)) is likely to be unstable to an LHD-like ballooning/interchange mode with ion Larmor radius scale lengths and ion cyclotron frequencies. Although tempting, it is certainly premature to identify the nearly continuous presence of turbulence in the center of the plasma sheet with the LHD-like mode. In addition, whether the ballooning/interchange modes significantly affect the plasma and flux transport in the plasma sheet remains to be determined, although the simulation results certainly indicate that under suitable conditions, the mode can grow to large amplitudes and produce macroscopic redistributions of the magnetic flux.

[45] **Acknowledgments.** This research was supported by National Science Foundation grant ATM-0352326. The particle simulations were performed using resources of the National Center for Supercomputing Applications Intel 64 Cluster Abe under grant ATM070016N and the University of Texas Advanced Computer Center Lonestar Cluster under grant ATM070016N.

[46] Amitava Bhattacharjee thanks the reviewer for the assistance in evaluating this paper.

References

Angelopoulos, V., W. Baumjohann, C. F. Kennel, F. V. Coroniti, M. G. Kivelson, R. Pellat, R. J. Walker, H. Lühr, and G. Paschmann (1992), Bursty bulk flows in the inner central plasma sheet, *J. Geophys. Res.*, *97*, 4027.

Asano, Y., T. Mukai, M. Hoshino, Y. Saito, H. Hayakawa, and T. Nagai (2003), Evolution of the thin current sheet in a substorm observed by Geotail, *J. Geophys. Res.*, *108*(A5), 1189, doi:10.1029/2002JA009785.

Asano, Y., T. Mukai, M. Hoshino, Y. Saito, H. Hayakawa, and T. Nagai (2004), Statistical study of thin current sheet evolution around substorm onset, *J. Geophys. Res.*, *109*, A05213, doi:10.1029/2004JA010413.

Baker, D. N., T. I. Pulkkinen, V. Angelopoulos, W. Baumjohann, and R. L. McPherron (1996), Neutral line model of substorms: Past results and present view, *J. Geophys. Res.*, *101*, 12,975.

Baumjohann, W., G. Paschmann, and H. Lühr (1990), Characteristics of high-speed ion flows in the plasma sheet, *J. Geophys. Res.*, *95*, 3801.

Bernstein, I. B., E. A. Frieman, M. D. Kruskal, and A. M. Kulsrud (1958), An energy principle for hydromagnetic stability problems, *Proc. R. Soc. London, Ser. A*, *244*, 17.

Birn, J., R. Sommer, and K. Schindler (1975), Open and closed magnetospheric tail configurations and their stability, *Astrophys. Space Sci.*, *35*, 389.

Büchner, J., and L. M. Zelenyi (1987), Chaotization of the electron motion as the cause of an internal magnetotail instability and substorm onset, *J. Geophys. Res.*, *92*, 13,456.

Chen, C. X., and R. A. Wolf (1993), Interpretation of high-speed flows in the plasma sheet, *J. Geophys. Res.*, *98*, 21,409.

Cheng, C. Z., and A. T. Y. Lui (1998), Kinetic ballooning instability for substorm onset and current disruption observed by AMPTE/CCE, *Geophys. Res. Lett.*, *25*, 4091.

Coroniti, F. V., and C. F. Kennel (1973), Can the ionosphere regulate magnetospheric convection?, *J. Geophys. Res.*, *78*, 2837.

Erickson, G. M. (1984), On the cause of X-line formation in the near-Earth plasma sheet: Results of adiabatic convection of plasma-sheet plasma, in *Magnetic Reconnection in Space and Laboratory Plasmas*, *Geophys. Monogr. Ser.*, vol. 30, edited by E. W. Hones Jr., p. 296, AGU, Washington, D.C.

Erickson, G. M. (1992), A quasi-static magnetospheric convection model in two dimensions, *J. Geophys. Res.*, *97*, 6505.

Erickson, G. M., and R. A. Wolf (1980), Is steady state convection possible in the Earth's magnetotail?, *Geophys. Res. Lett.*, *7*, 897.

Fairfield, D. H. (1986), The magnetic field of the equatorial magnetotail from 10 to 40 R_E, *J. Geophys. Res.*, *91*, 4238.

Harris, E. G. (1962), On a plasma sheath separating regions of oppositely directed magnetic field, *Nuovo Cimento*, *23*, 115.

Hau, L.-N. (1991), Effects of steady state adiabatic convection on the configuration of the near-Earth plasma sheet, 2, *J. Geophys. Res.*, *96*, 5591.

Hau, L.-N., R. A. Wolf, G.-H. Voigt, and C. C. Wu (1989), Steady state magnetic field configurations for the Earth's magnetotail, *J. Geophys. Res.*, *94*, 1303.

Huba, J. D., J. G. Lyon, and A. B. Hassam (1987), Theory and simulation of the Rayleigh Taylor instability in the large Larmor radius limit, *Phys. Rev. Lett.*, *59*, 2971.

Hurricane, O. A., R. Pellat, and F. V. Coroniti (1995), A new approach to low-frequency "MHD-like" waves in magnetospheric plasmas, *J. Geophys. Res.*, *100*, 19,421.

Hurricane, O. A., R. Pellat, and F. V. Coroniti (1996), Instability of the Lembège-Pellat equilibrium under ideal magnetohydrodynamics, *Phys. Plasmas*, *3*, 2472.

Lembège, B., and R. Pellat (1982), Stability of a thick two-dimensional quasineutral sheet, *Phys. Fluids*, *25*, 1995.

Lui, A. T. Y. (1996), Current disruption in the Earth's magnetosphere: Observations and models, *J. Geophys. Res.*, *101*, 13,067.

Mitchell, D. G., D. J. Williams, C. Y. Huang, L. A. Frank, and C.T. Russell (1990), Current carriers in the near-Earth cross tail current sheet during substorm growth phase, *Geophys. Res. Lett.*, *15*, 583.

Mozer, F. S., S. D. Bale, and T. D. Phan (2002), Evidence of diffusion regions at a subsolar magnetopause crossing, *Phys. Rev. Lett.*, *89*, 015002.

Pontius, D. H., Jr., and R. A. Wolf (1990), Transient flux tubes in the terrestrial magnetosphere, *Geophys. Res. Lett.*, *17*, 49.

Pritchett, P. L. (2000), Particle-in-cell simulations of magnetosphere electrodynamics, *IEEE Trans. Plasma Sci.*, *28*, 1976.

Pritchett, P. L. (2002), Simulation of cross-field instabilities in a current sheet for more realistic values of the ion to electron mass ratio, in *Sixth International Conference on Substorms*, edited by R. M. Winglee, p. 225, Univ. of Wash., Seattle, Wash.

Pritchett, P. L., and J. Büchner (1995), Collisionless reconnection in configurations with a minimum in the equatorial magnetic field and with magnetic shear, *J. Geophys. Res.*, *100*, 3601.

Pritchett, P. L., and F. V. Coroniti (1990), Plasma sheet convection and the stability of the magnetotail, *Geophys. Res. Lett.*, *17*, 2233.

Pritchett, P. L., and F. V. Coroniti (1995), Formation of thin current sheets during plasma sheet convection, *J. Geophys. Res.*, *100*, 23,551.

Pritchett, P. L., and F. V. Coroniti (1997), Interchange and kink modes in the near-Earth plasma sheet and their associated plasma flows, *Geophys. Res. Lett.*, *24*, 2925.

Pritchett, P. L., and F. V. Coroniti (1998), Interchange instabilities and localized high-speed flows in the convectively-driven near-Earth plasma sheet, in *Substorms-4*, edited by S. Kokubun and Y. Kamide, p. 443, Springer, New York.

Pritchett, P. L., F. V. Coroniti, R. Pellat, and H. Karimabadi (1991), Collisionless reconnection in two-dimensional magnetotail equilibria, *J. Geophys. Res.*, *96*, 11,523.

Pritchett, P. L., F. V. Coroniti, and V. K. Decyk (1996), Three-dimensional stability of thin quasi-neutral current sheets, *J. Geophys. Res.*, *101*, 27,413.

Pritchett, P. L., F. V. Coroniti, and R. Pellat (1997), Convection-driven reconnection and the stability of the near-Earth plasma sheet, *Geophys. Res. Lett.*, *24*, 873.

Pulkkinen, T. I., and M. Wiltberger (2000), Thin current sheet evolution as seen in observations, empirical models and MHD simulations, *Geophys. Res. Lett.*, *27*, 1363.

Pulkkinen, T. I., D. N. Baker, D. G. Mitchell, R.L. McPherron, C. Y. Huang, and L. A. Frank (1994), Thin current sheets in the magnetotail during substorms: CDAW 6 revisited, *J. Geophys. Res.*, *99*, 5793.

Rosenbluth, M. N., and C. L. Longmire (1957), Stability of plasmas confined by magnetic fields, *Ann. Phys.*, *1*, 120.

Saito, M. H., Y. Miashita, M. Fujimoto, I. Shinohara, Y. Saito, K. Liou, and T. Mukai (2008a), Ballooning mode waves prior to substorm-associated dipolarizations: Geotail observations, *Geophys. Res. Lett.*, *35*, L07103, doi:10.1029/2008GL033269.

Saito, M. H., Y. Miashita, M. Fujimoto, I. Shinohara, Y. Saito, and T. Mukai (2008b), Modes and characteristics of low-frequency MHD waves in the near-Earth magnetotail prior to dipolarization: Fitting method, *J. Geophys. Res.*, *113*, A06201, doi:10.1029/2007JA012778.

Sanny, J., R. L. McPherron, C. T. Russell, D. N. Baker, T. I. Pulkkinen, and A. Nishida (1994), Growth-phase thinning of the near-Earth current sheet during the CDAW 6 substorm, *J. Geophys. Res.*, *99*, 5805.

Schindler, K. (1972), A self-consistent theory of the tail of the magnetosphere, in *Earth's Magnetospheric Processes*, edited by B. M. McCormac, p. 200, D. Reidel, Norwell, Mass.

Schindler, K., and J. Birn (1982), Self-consistent theory of time-dependent convection in the Earth's magnetotail, *J. Geophys. Res.*, *87*, 2263.

Sergeev, V. A., D. G. Mitchell, C. T. Russell, and D. J. Williams (1993), Structure of the tail plasma/current sheet at ~11R_E and its changes in the course of a substorm, *J. Geophys. Res.*, *98*, 17,345.

Sergeev, V. A., T. I. Pulkkinen, R. J. Pellinen, and N. A. Tsyganenko (1994), Hybrid state of the tail magnetic configuration during steady convection events, *J. Geophys. Res.*, *99*, 23,571.

Sitnov, M. I., P. N. Guzdar, and M. Swisdak (2005), On the formation of a plasma bubble, *Geophys. Res. Lett.*, *32*, L16103, doi:10.1029/2005GL023585.

Sitnov, M. I., P. N. Guzdar, and M. Swisdak (2007), Atypical current sheets and plasma bubbles: A self-consistent kinetic model, *Geophys. Res. Lett.*, *34*, L15101, doi:10.1029/2007GL029693.

Winske, D. (1996), Regimes of the magnetized Rayleigh-Taylor instability, *Phys. Plasmas*, *3*, 3966.

Wygant, J. R., et al. (2005), Cluster observations of an intense normal component of the electric field at a thin reconnecting current sheet in the tail and its role in the shock-like acceleration of the ion fluid into the separatrix region, *J. Geophys. Res.*, *110*, A09206, doi:10.1029/2004JA010708.

Yee, K. S. (1966), Numerical solution of initial boundary value problems involving Maxwell's equations in isotropic media, *IEEE Trans. Antennas Propag.*, *14*, 302.

F. V. Coroniti and P. L. Pritchett, Department of Physics and Astronomy, University of California, 405 Hilgard Avenue, Los Angeles, CA 90095-1547, USA. (pritchet@physics.ucla.edu)